Energy and Buildings 130 (2016) 829–842

Contents lists available at ScienceDirect

Energy and Buildings

journal homepage: www.elsevier.com/locate/enbuild

Intra-urban differences of mean radiant temperature in different urban settings in Shanghai and implications for heat stress under heat waves: A GIS-based approach

Liang Chen[a,*], Bailang Yu[a,b], Feng Yang[c,d], Helmut Mayer[e]

[a] School of Geographic Sciences, East China Normal University, Shanghai, China
[b] Key Laboratory of Geographic Information Science, Ministry of Education, East China Normal University, Shanghai, China
[c] College of Architecture and Urban Planning (CAUP), Tongji University, Shanghai, China
[d] Key Laboratory of Ecology and Energy-Saving Study of Dense Habitat, Tongji University, Ministry of Education, China
[e] Chair of Environmental Meteorology, Albert-Ludwigs-University of Freiburg, Germany

ARTICLE INFO

Article history:
Received 1 August 2016
Received in revised form 4 September 2016
Accepted 6 September 2016
Available online 9 September 2016

Keywords:
Mean radiant temperature
SOLWEIG
Heat stress
Shanghai

ABSTRACT

The mean radiant temperature (T_{mrt}) is an effective indicator to characterize the urban thermal radiant environment and assess outdoor thermal comfort and heat stress. In this study, the SOLWEIG model (SOlar and Long Wave Environmental Irradiance Geometry) was employed to investigate the spatial variation of T_{mrt} in different urban settings in Shanghai. The model was tested against six directional radiant flux density measurements and showed good performance in Shanghai's urban environment. Two different urban settings with different building geometry and vegetation cover were used as case study sites. A typical heat wave day in 2013 was selected to investigate the daytime radiant heat stress intensity. Spatial analysis modules were developed and the Radiant Heat Stress Intensity index was defined. The study reveals that in Shanghai under heat waves the heat stress induced by the thermal radiant environment is quite severe, with T_{mrt} commonly well above 60 °C in daytime, and intra-urban T_{mrt} differences are largely influenced by building density and height, street orientation and vegetation. Open paved spaces and space near sunlit walls are the places that have the highest T_{mrt}. The study shows that the spatial variation of T_{mrt} can be used to identify thermally vulnerable areas and hotspots in complex urban environment, and provide implications for urban design towards the mitigation of heat stress in high-density cities.

1. Introduction

Heat stress in cities is becoming increasingly severe due to the unprecedented urbanization and global warming paces. Urban overheating not only has large impacts on the energy consumption in buildings [1–3], but also significantly affects outdoor thermal comfort and therefore citizen's behavior and lifestyle [4]. With respect to people's comfort, health and well-being, daytime heat stress will cause health risks such as fatigue, morbidity, or even mortality in extreme weather conditions such as heat waves [5–7].

Besides the high air temperature in city centers which has been commonly observed and widely studied [8,9], the thermal radiant aspect of the urban environment has drawn much attention only in recent years with the progress in remote sensing technologies and in-situ monitoring techniques. In fact, convective fluxes of sensible heat and latent heat are more significant in directing human energy balance and thermoregulation as compared to conductive heat, especially in strong solar exposure conditions. Therefore the thermal radiant environment plays a more important role in affecting outdoor thermal comfort in hot summer. There have been an increasing number of research studies aiming at mitigating urban heat island and reducing heat stress in cities from the thermal radiant perspective [10–12]. Comprehensive reviews have also been conducted on the state-of-the-art technologies to mitigate UHI, especially from the thermal comfort aspect, such as the development of reflective materials, cool roof and pavement, and urban greening [13,14].

The mean radiant temperature (T_{mrt}) is the most important meteorological parameter that characterizes the effect of thermal radiant environment on human thermal comfort [15]. It is defined

* Corresponding author.
E-mail address: lchen@geo.ecnu.edu.cn (L. Chen).

http://dx.doi.org/10.1016/j.enbuild.2016.09.014
0378-7788/

as "the uniform temperature of an imaginary enclosure in which the radiant heat transfer from the human body equals the radiant heat transfer in the actual non-uniform enclosure" [16]. By definition, T_{mrt} parameterizes the holistic effect of the complex radiation fluxes of the thermal radiant environment into a single temperature-dimension index (°C). In a complex urban environment, the radiation fluxes vary considerably in outdoor spaces because of the shading generated by buildings and vegetation, and also because of different surface materials. Therefore T_{mrt} can exhibit significant spatial variation even within a short distance. For example, Mayer and Höppe [17] showed through in-situ meteorological measurement that the T_{mrt} difference between a sunlit street canyon and a nearby shaded street canyon can be up to 30 °C in the early afternoon, whereas the difference of the air temperature (T_a) is less than 3 °C. This suggests that T_{mrt} can be a more suitable index for characterizing the intra-urban differences of thermal comfort conditions as compared to traditional meteorological indices such as T_a, especially in complex urban environment. Therefore T_{mrt} has been widely adopted across the world in urban human-biometeorological studies to parameterize the level of thermal comfort and heat stress in hot summer [18–23]. Thorsson et al. [24] also found that T_{mrt} can effectively predict the risk of mortality of senior citizens induced by heat stress.

In urban outdoor spaces, T_{mrt} is primary determined by building geometry, street layout, albedo of facade and ground, and vegetation cover. These components can be effectively altered by design interventions. Therefore understanding how the spatial variation of T_{mrt} is affected by different urban settings is important and can provide valuable implications for climate-responsive urban design and planning. An increasing number of studies have hence addressed this concern across different scales, including micro scale such as street canyons [25–27] and urban open spaces [28], neighborhood scale such as residential communities [29], and district scale with various building shapes and street orientations [30–34]. It is commonly found that building geometry and vegetation plays the most significant role in affecting T_{mrt} and thus the overall thermal comfort [25,27,35,36], in contrast the contribution of surface albedo is rather minor [37,38]. So far most of the studies were carried out in urban environment with low or moderate density, such as mid-size European cities [27,33,36]. In the high-density urban environment of a metropolitan such as Shanghai, the spatial variation of T_{mrt} is further complexed by the combination of deep street canyons, shadow casted by high-rise buildings, near-wall sunlit spaces, etc. Lau et al. [39] took the downtown center of Hong Kong as an example and addressed the issue in high-density urban environment. On the other hand the discussion was qualitative rather than analytical. No quantitative comparisons were given for the spatial variation of T_{mrt} of the selected "open area" and "denser area" which are separated by a road, and no vegetation was included in the estimation of T_{mrt} even though there were urban parks and green spaces, which are also essential urban elements. Furthermore the use of summer average weather data may be less revealing since Thorsson et al. [24] have shown that daily maximum T_{mrt} can better reflect the level of heat stress as indicated by mortality.

The objective of the present study is to investigate the spatial variation of T_{mrt} as affected by different urban geometry and vegetation in high-density cities and its implication for heat stress during heat waves. Two different urban settings in Shanghai's downtown area were selected as the study sites. The Solar and Long Wave Environmental Irradiance Geometry (SOLWEIG) model [35,40] was validated with field measurement and used to simulate T_{mrt} pattern for a real summer hot day to examine the actual meteorological conditions. The index of *Radiant Heat Stress Intensity* (RHSI) was defined to evaluate heat stress intensity from the thermal radiant aspect. Spatial analysis of the spatial variations of T_{mrt} was conducted, based on which heat stress areas were identified and urban design implications for mitigating urban heat stress were proposed.

2. Methods

2.1. Study area

Shanghai (30°40′N ~31°53′N, 120°51′E ~122°12′E), the biggest city in China, is located on the alluvial terrace of the Yangtze River delta with average elevation of 4 m above sea level. It has a northern subtropical monsoon climate, with a mean annual T_a of 17.2 °C, and monthly maximum and minimum mean T_a of 30.2 °C in July and 1.9 °C in January for the last 30 years, respectively. The city's administrative boundaries cover a total terrestrial area of 6340.5 km^2 excluding estuary waters. The city has a total population of 24.15 million, including both permanent and non-permanent residents. As one of the most rapidly urbanizing cities in China, Shanghai is also suffering increasingly severe heat stress. In 2013, the city experienced its hottest summer in the last 140 years since weather data was recorded. Eight consecutive days of T_a above 38 °C and 25 days of T_a above 35 °C were recorded in July. The highest official T_a of 40.6 °C was also recorded by the city's benchmark observatory. During the hot spell, hospital admissions generally increased by 30%, and at least 10 people died from heat stroke [41,42]. In such cases, identifying urban hot spots and areas vulnerable to heat stress is particularly important for implementing alerting and protection measures.

The Lujiazui (LJZ) central business district is located in the Pudong New District on the eastern bank of the Huangpu River just across the Bund. The area has a mixture of commercial, business and high-end residential land uses. There are a total number of 45 super high-rise buildings taller than 200 m in LJZ, and the tallest building, Shanghai Center, is 632 m high. The area is also characterized by abundant urban open spaces and greenery including parks and roadside trees. In comparison, the old residential neighborhood of Xiaonanmen (XNM) is located in the Huangpu District on the western bank of the Huangpu River. The area is densely packed with old residential buildings normally 1–4 story high. Although there are a few tall buildings built more recently, none of them is taller than 120 m. Because of the limited space, vegetation such as trees and shrubs is extremely scarce in XNM, and in some narrow streets there is literally no urban greenery. The area is also dominated by the regular E-W and N-S street orientations. These two areas represent two different urban settings of the high-dense city center of Shanghai. Fig. 1 shows the locations of LJZ and XNM in Shanghai and snapshots of their typical street scenarios. Two 1 km by 1 km sites were selected from LJZ and XNM as case study sites. Fig. 2 shows the digital elevation model (DEM). Table 1 summarizes the morphological information of the two sites.

2.2. SOLWEIG model: validation and simulation

The SOLWEIG model (SOlar and Long Wave Environmental Irradiance Geometry) [35,40] is a computational model that can simulate the spatial variation of T_{mrt} in a complex urban environment. SOLWEIG calculates T_{mrt} by simulating the 3-D radiant flux densities of the surrounding environment, which is based on the integral 3-D radiant environment monitoring technique proposed by Höppe [19]. The monitoring method has been considered as the most accurate way to determine T_{mrt} values in outdoor environment [43]. SOLWEIG rebuilds the measurement procedures in a virtual sense, i.e. simulating the shortwave and longwave radiant flux densities from the six directions of the surrounding environment (east, west, north, south, upward and downward) and estimating angular factors (proportion of radiation received by the

Fig. 1. Left: Locations of downtown center in Shanghai along the Huangpu River. Middle: Satellite image showing the study sites of LJZ (indicated by the red square on the top) and XNM (indicated by the red square at the bottom). Right: Typical street scenarios in LJZ (up) and XNM (down). (For interpretation of the references to color in this figure legend, the reader is referred to the web version of this article.)

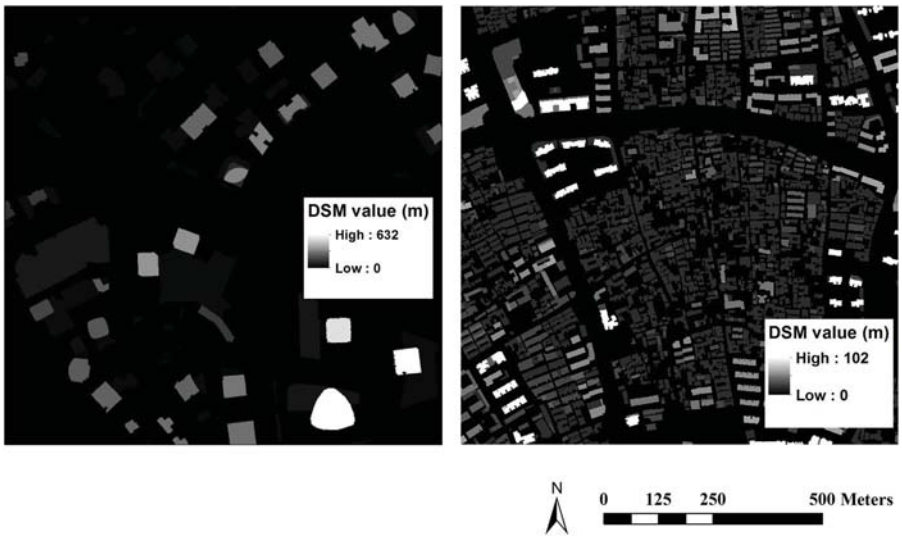

Fig. 2. DEM maps of LJZ (left) and XNM (right).

Table 1
Comparison of statistics of morphological information of LJZ and XNM.

Site	Total building floor area (10^6 m^2)	Built-up ratio (%)	Average building height (m)	Average SVF (sky view factor)/standard deviation
LJZ	4.82	18.0	107.1	0.65/0.17
XNM	1.46	36.5	12.9	0.53/0.21

human body in each direction). The model uses a digital surface model (DSM) as primary input data and implements fast algorithms for raster calculation. In this way it can deal with the real urban environment and calculate T_{mrt} values for a large spatial domain in a computationally efficient manner. Therefore SOLWEIG has advantages over other computer models that either are too time consuming such as the holistic simulating package of ENVI-met [44], or can only handle the point of interest such as RayMan [45]. SOLWEIG has been tested in a number of cities with various urban context and different climates [35,39,40,46]. Constant improvements have been made to the model, such as including the effect of vegetation [35] and surface material [38]. In this study, the latest version of SOLWEIG 2015a is used, which requires meteorological data consisting of time-series of T_a, relative humidity (RH) and global solar radiation (G), as well as DSMs of building and vegetation.

2.2.1. Model validation

To validate the SOLWEIG model in Shanghai's unique climatic context, 3-D radiant flux density monitoring campaigns were conducted in the university campus on two clear hot summer days, i.e. 17th and 25th, August 2015. Two cases were tested. One is a paved open square in the west of an N-S aligned building with limited vegetation on the western side (square case), the other is an E-W

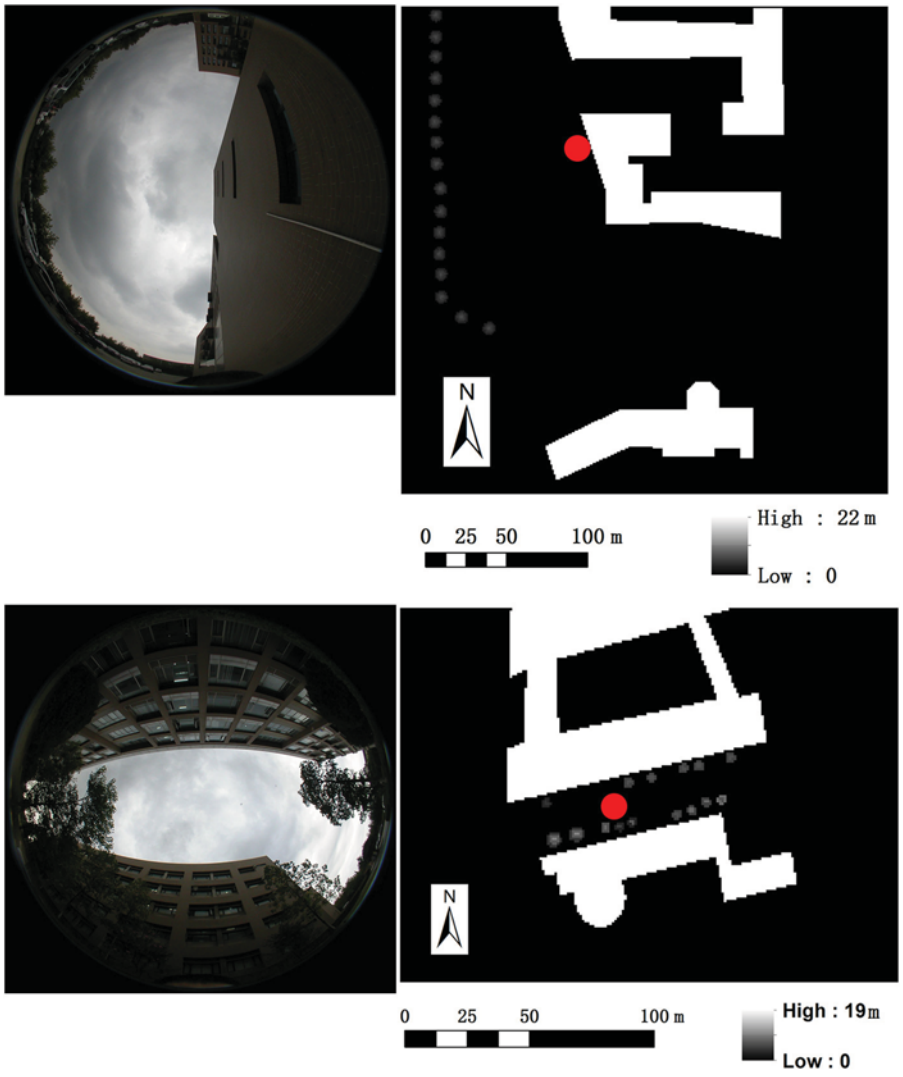

Fig. 3. Left: fish-eye lens photos taken at the measurement point in the square case (up) and the street canyon case (down). Right: DSMs of two validation sites, i.e. square case (up) and street canyon case (down), the red dots indicate the location of the measurement points and points of interest in SOLWEIG. (For interpretation of the references to color in this figure legend, the reader is referred to the web version of this article.)

Table 2
Input data and parameter settings for SOLWEIG simulation.

	Required input	Data/Value
Meta data	Building data	Building DEM, 1 m resolution
	Vegetation data	Vegetation DSM, 1 m resolution
	Weather data	15 min time series of T_a, RH and G
Urban parameters	Building surface albedo	0.2
	Ground surface albedo	0.2
	Emissivity of building walls	0.9
	Emissivity of ground surface	0.95
	Transmissivity of shortwave radiation through trees	0.05
	Transmissivity of longwave radiation through trees	0
Personal parameters	Absorption coefficients for shortwave radiation	0.7
	Absorption coefficients for longwave radiation	0.97
	Posture	Standing

oriented street canyon with much vegetation (street canyon case). The two selected sites can be used to evaluate SOLWEIG's performance in near-wall and open space cases, street canyon, and also cases when vegetation is included. One set of net radiometer (Kipp & Zonen CNR 4) was used to measure the 3-D radiant flux densities. The radiometer was rotated every 3 min to each of the three directions (E-W, N-S, U-D). The monitoring was conducted from 8:00 to 16:00 for each day, following standard measurement routines proposed by [19,43]. SOLWEIG simulations were performed for the two days, and compared with field measurement data for model validation. Fig. 3 shows the fish-eye lens photographs taken at the measurement points and the DSMs showing the point of interest used for validation. Table 2 summarizes the input data and parameter settings of the SOLWEIG simulation.

2.2.2. Simulation of T_{mrt} in two urban sites

SOLWEIG simulations were performed for the two selected sites in downtown Shanghai. One clear and calm hot summer day in a heat wave, i.e. July 28, 2013 was selected for investigation. Meteorological data recorded by meteorological stations of the Shanghai Meteorological Bureau were used to simulate the real case of the spatial variation of T_{mrt}. There is a station located in the center of LJZ, and another station located about 2 km to the west of XNM. Normally T_a for XNM is 2–3 °C higher than LJZ in summer daytime primarily due to the high density. For the simulation day, the maximum T_a was 38.7 °C and 40.1 °C for LJZ and XNM, respectively. Fig. 4 shows the hourly variation of major meteorological parameters for the two sites on the simulation day.

Building DSMs were generated from 3-D building database acquired from Shanghai Institute for Surveying and Mapping, with the resolution of 1m. Vegetation DSM for LJZ was generated from airborne LiDAR data [47], which was further corrected and supplemented by on-site surveys based on the profile of greenery provided by Google Map satellite images. Standard absorption coefficients for shortwave and longwave radiation were used, i.e. 0.7 and 0.97, respectively [19]. The surface albedo for building and ground surfaces was set to 0.2. The emissivity of building walls was set to 0.9 representing a combination of concrete and glass, and the emissivity of ground surfaces was set to 0.95 for rough concrete. The transmissivity of shortwave and longwave radiation through vegetation was set to 0.05 and 0, respectively, as recommended by [35]. Base on the input DSMs, meteorological data, surface characteristics, and Shanghai's geographical location, T_{mrt} values were calculated for a standing or walking person, using the surface projection factors of 0.22 for the east, west, north and south directions, and 0.06 for the upward and downward directions [17,19,23]. The simulations were conducted for each hour from 9:00 to 16:00.

3. Results and analysis

3.1. Model performance

Modeled shortwave and longwave radiant flux densities at 15 min interval from 09:00 to 16:00 were compared with measurement data. Downward, upward, side and total shortwave and longwave radiant flux densities were compared, denoted as K_{down}, K_{up}, K_{side}, K_{total} for shortwave, and L_{down}, L_{up}, L_{side}, L_{total} for longwave, which is also the settings used by [39,40]. Figs. 5 and 6 show the correlations between modeled and measured shortwave and longwave radiant flux densities for the square case and street canyon case, respectively. As the figures show, the performance of the SOLWEIG model is very good. For the square case when little vegetation is present, SOLWEIG can explain 96.2% of the variance in K_{total} (RMSE = 130.7 W/m^2) and 95.6% of the variance in L_{total} (RMSE = 41.4 W/m^2). For the street canyon case when a lot of vegetation is present, SOLWEIG can explain 94.7% of the variance in K_{total} (RMSE = 142.2 W/m^2) and 85.3% of the variance in L_{total} (RMSE = 43.0 W/m^2). Table 3 summarizes the correlation results.

More careful examinations were given to different components of K_{total} and L_{total} to evaluate model performance in detail. For the square case, the modeled K_{down} and K_{up} agreed with measured values very well, i.e. R^2 = 0.93, RMSE = 60.9 W/m^2 for K_{up}, and R^2 = 0.92, RMSE = 14.4 W/m^2 for K_{down}. The good correlation was expected, as the calculation of these two components was straightforward based on input radiation data and sky obstruction. For the lateral directions, noticeably SOLWEIG underestimated K_{east}, with R^2 = 0.83, and RMSE = 31.8 W/m^2. This was especially the case when the building wall which was very close (~2 m) to the east of the measurement point got sunlit in the early afternoon, and high near-wall shortwave fluxes were observed that could be up to 70 W/m^2 higher than modeled values. This discrepancy was believed to be caused by high reflection from building surfaces. SOLWEIG also overestimated K_{west}, with R^2 = 0.81 and RMSE = 83.6 W/m^2, especially after 11:00 when the sun was visible, and the overestimation was believed to be caused by the lack of building and vegetation data in the west direction outside the campus. K_{south} was slightly overestimated, with R^2 = 0.87 and RMSE = 29.9 W/m^2, which was caused by not considering trees to the south of the site. On the other hand, K_{north} was estimated very accurately, with R^2 = 0.91 and RMSE = 7.1 W/m^2, because buildings and trees outside the site were far away, thus had little influence on the measurement point. For longwave radiation, SOLWEIG can also simulate longwave radiant fluxes very well, i.e. L_{down}: R^2 = 0.89, RMSE = 8.3 W/m^2; L_{up}: R^2 = 0.96, RMSE = 9.0 W/m^2; L_{south}: R^2 = 0.96, RMSE = 6.1 W/m^2; L_{north}: R^2 = 0.93, RMSE = 9.5 W/m^2; L_{east}: R^2 = 0.84, RMSE = 11.4 W/m^2; L_{west}: R^2 = 0.95, RMSE = 7.5 W/m^2. The biggest discrepancy was found for L_{east} (near-wall case), and SOLWEIG constantly underestimated L_{east} by over 20 W/m^2 when the wall got sunlit. This underestimation conflicts with findings reported in [40]. Since the distance to the nearby wall was not specified in the paper, the cause of such disagreement could not be further examined. Nevertheless, future work should address the near-wall case in detail.

Table 3
Summary of the validation results for the two cases.

	Square case		Street canyon case	
	R^2	RMSE (W/m^2)	R^2	RMSE (W/m^2)
K_{up}	0.93	60.9	0.86	14.7
K_{down}	0.92	14.4	0.91	65.0
K_{side}	0.91	128.3	0.92	103.7
K_{total}	0.96	130.7	0.95	142.2
L_{up}	0.96	9.0	0.88	12.3
L_{down}	0.89	8.3	0.80	5.5
L_{side}	0.95	28.7	0.73	35.3
L_{total}	0.96	41.4	0.85	43.0

For the street canyon case, SOLWEIG simulated both shortwave and longwave radiant flux densities considerably well, but with relatively lower R^2 as compared to the square case (K_{down}: R^2 = 0.91, RMSE = 65.0 W/m^2; K_{up}: R^2 = 0.86, RMSE = 14.7 W/m^2; K_{side}: R^2 = 0.92, RMSE = 103.7 W/m^2; L_{down}: R^2 = 0.88, RMSE = 5.5 W/m^2; L_{up}: R^2 = 0.86, RMSE = 12.3 W/m^2; L_{side}: R^2 = 0.79, RMSE = 35.3 W/m^2). The reason for the lower correlation is because the irregular shape of tree trunks cannot be fully parameterized in the model. Noticeably modeled K_{north} and K_{south} showed lowest correlations with measurement data, with R^2 = 0.65 and RMSE = 19.8 W/m^2 for K_{north}, as well as R^2 = 0.71 and RMSE = 41.8 W/m^2 for K_{south}. Because the study site is an E-W oriented street canyon, the discrepancy could be attributed to the reflection from building surfaces. In the case of K_{south}, when the building facade got sunlit at noon time, measured value could be over 40 W/m^2 higher than modeled value.

Fig. 7 shows the comparisons between measured and modeled T_{mrt} values for a standing person based on the flux density data for the two cases. The figure reveals that modeled T_{mrt} values showed good agreement with measured values, with R^2 higher than 0.9. Noticeably, in the early afternoon with strong shortwave radiation reflected from building facades, SOLWEIG tended to underestimate T_{mrt} by around 3 °C for the near wall case. Other than that SOLWEIG normally overestimated T_{mrt} by around 4 °C, which could be attributed to the overestimated lateral longwave radiant fluxes, which is consistent with findings reported in [39,40]. The comparisons proved that with accurate input data of building morphology and vegetation cover, SOLWEIG can accurately simulate the spa-

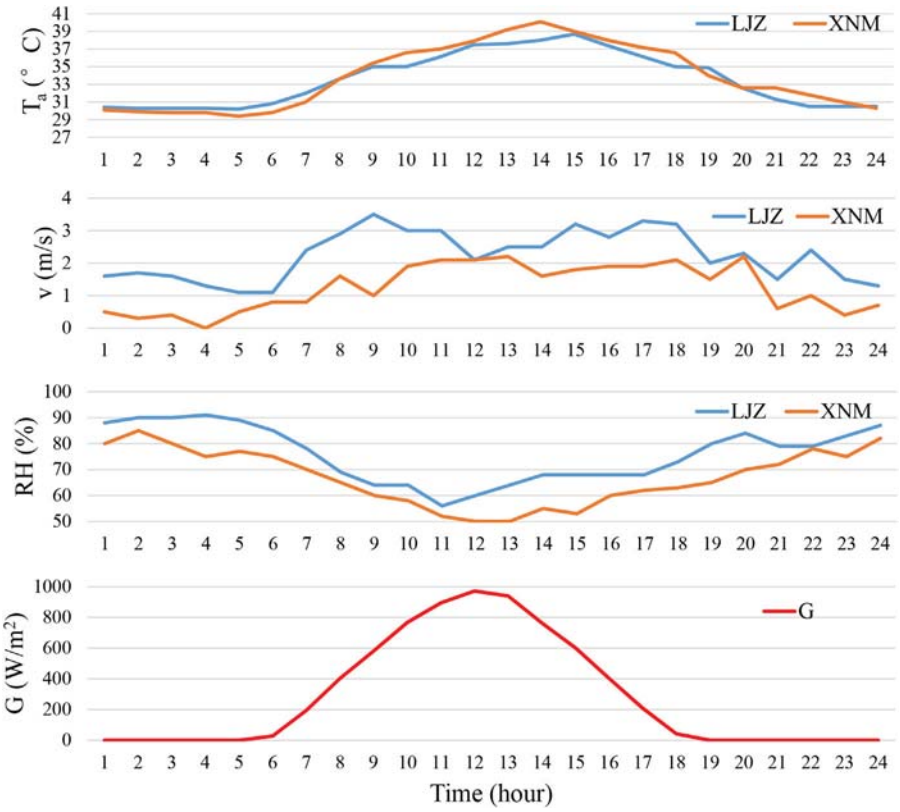

Fig. 4. Hourly variation of major meteorological parameters for both sites on July 28, 2013: air temperature (Ta), wind speed (v), relative humidity (RH), and global radiation (G).

tial variation of T_{mrt} in various urban settings. The applicability of SOLWEIG in Shanghai's climatic context was therefore validated.

3.2. Spatio-temporal variations of T_{mrt} in two urban settings on a hot day

Figs. 8 and 9 show the hourly spatial variations of T_{mrt} for the two selected sites in downtown Shanghai, i.e. LJZ and XNM on July 28, 2013 from 11:00 to 15:00, representing the hottest time of a day. Table 4 summarizes the statistics of T_{mrt} values in the two sites. It is shown that on a hot day, daytime T_{mrt} in Shanghai's urban center is very high in general, normally well above 40 °C even in shaded areas. During the study period, both sites showed similar temporal pattern of T_{mrt} changes: at 11:00, the solar radiation is already very high (~890 W/m^2), and because of the high T_a (above 36 °C), T_{mrt} can be over 70 °C in sunlit areas and 40 °C in shaded areas. As T_a keeps increasing and solar radiation is constantly above 800 W/m^2, T_{mrt} reaches its maximum value at 14:00. For LJZ, maximum T_{mrt} of 84.4 °C was found at the paved open square near waterfront in the northwest of the site, primarily due to the extremely high shortwave radiation reaching and reflected from the ground. In the meantime, minimum T_{mrt} of 50.8 °C was found at the deep shadow casted by high buildings and trees.

For XNM, because the local T_a can be up to 2 °C higher than LJZ, therefore T_{mrt} can be considerably higher than 80 °C in some extreme cases. Maximum T_{mrt} of 90.0 °C was found near the south-facing wall in the wide E-W road in the center of the site, which is the result of intense shortwave and longwave radiations both from the ground and the wall. In fact in the sunlit locations of this road, T_{mrt} values all exceed 87 °C. Meanwhile minimum T_{mrt} of 52.1 °C was found at the western side of the shaded N-S street canyon in the densely built up areas in the center of the site. It is noticeable that LJZ shows a much more diverse spatial distribution of T_{mrt} as compared to XNM, with standard deviation commonly above 10 °C during the study period, in contrast XNM's standard deviation of T_{mrt} is normally around 5–6 °C. The difference is also reflected in the local scale. For example, in LJZ, for a tall building with a large open paved space in the south, the T_{mrt} values in front of the south-facing wall of the building could be over 30 °C higher than the T_{mrt} values in the deep shadow in the northwest of building. In comparison, in XNM, T_{mrt} values in shaded street canyons are normally around 15 °C lower than the nearby open space or center of wide roads, meanwhile T_{mrt} values in the northern sunlit side of E-W street canyons are normally 5–7 °C higher than T_{mrt} values in the western shaded side of nearby N-S street canyons. Nevertheless, the difference of T_{mrt} between different locations across the site can be above 35 °C during the study period for both LJZ and XNM, which is consistent with the 30 °C range as shown by [17].

4. Discussions

4.1. Intra-urban differences of T_{mrt} in Shanghai: effect of urban geometry

In order to focus on the spatial variations of T_{mrt} and examine the intra-urban differences of T_{mrt} in the two different urban settings in Shanghai, average T_{mrt} values from 11:00 to 15:00 were calculated. Fig. 10 shows the average hourly T_{mrt} values from 11:00 to 15:00 in LJZ and XNM. Fig. 11 shows the histograms of the T_{mrt} values in two maps. It is found that in LJZ, maximum average T_{mrt} of 82.0 °C occurred at the center of the paved open square near waterfront in the northwest of the site, which was in constant sun exposure from 11:00 to 15:00 and received extremely high longwave and shortwave radiation from the sky and also reflected from the ground. In other unobstructed spaces, average T_{mrt} values were normally below 80 °C, because of the shadow casted by nearby buildings

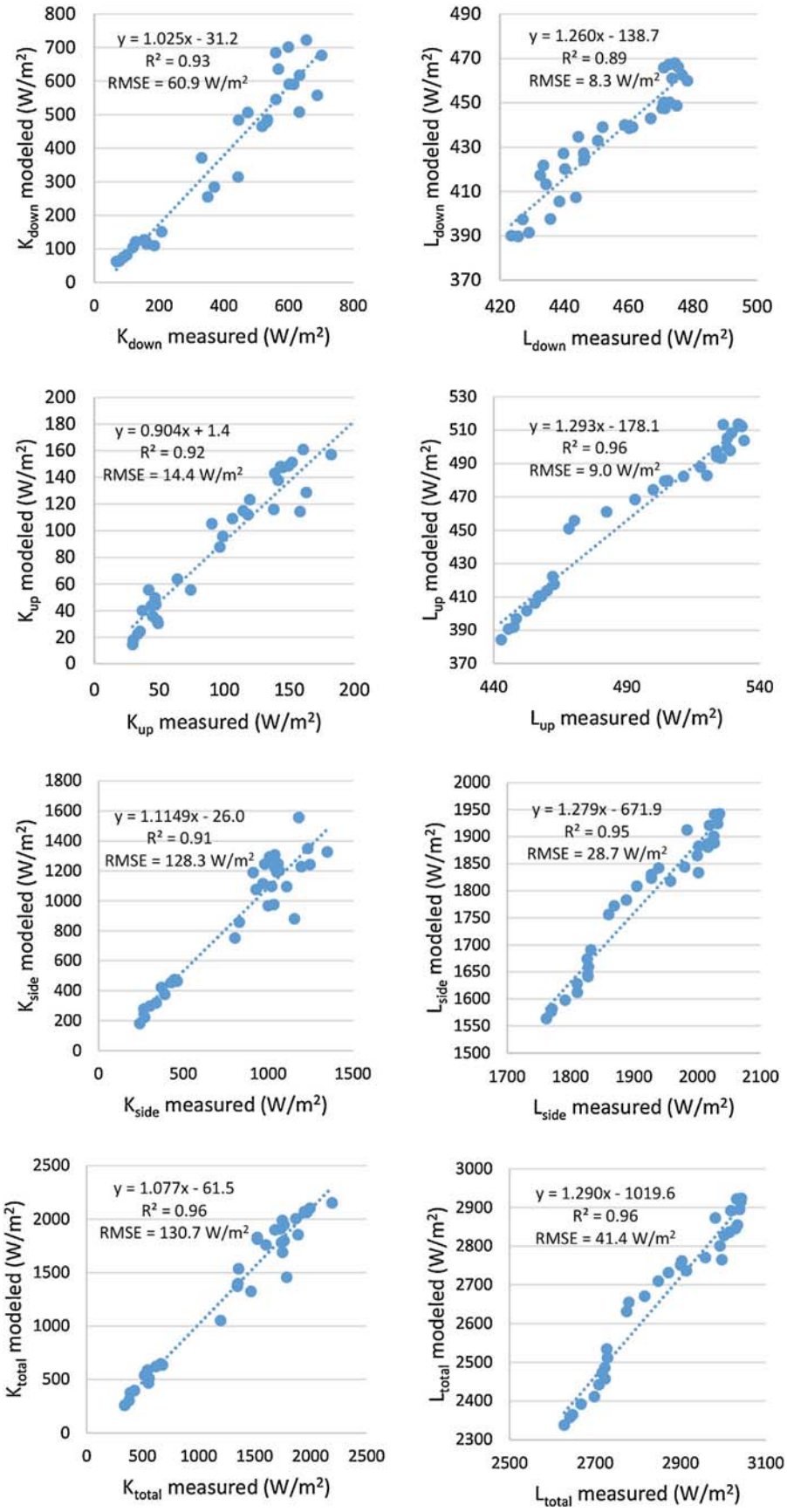

Fig. 5. Correlations between modeled and measured shortwave and longwave radiant flux densities at the measurement site for the square case.

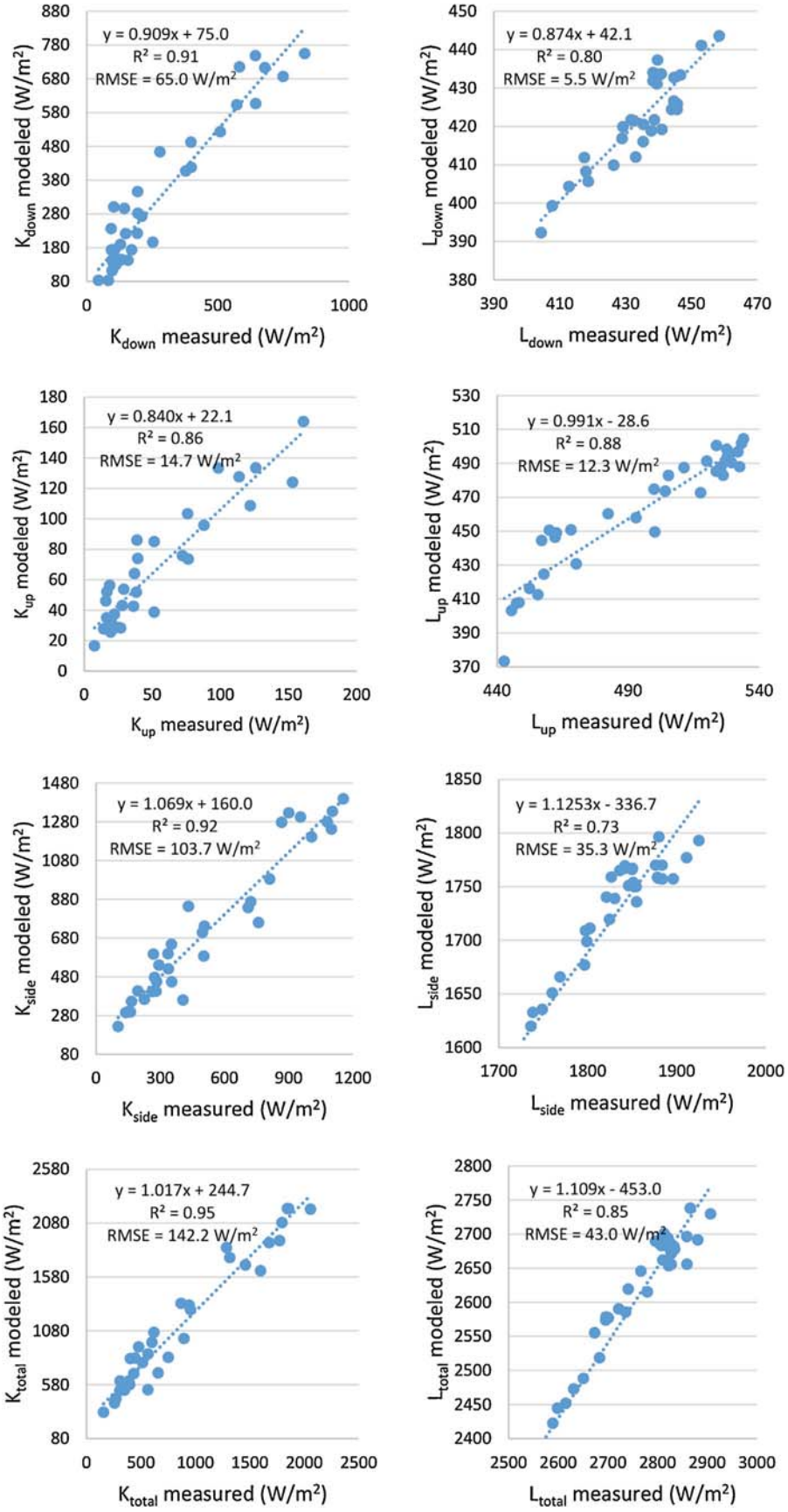

Fig. 6. Correlations between modeled and measured shortwave and longwave radiant flux densities at the measurement site for the street canyon case.

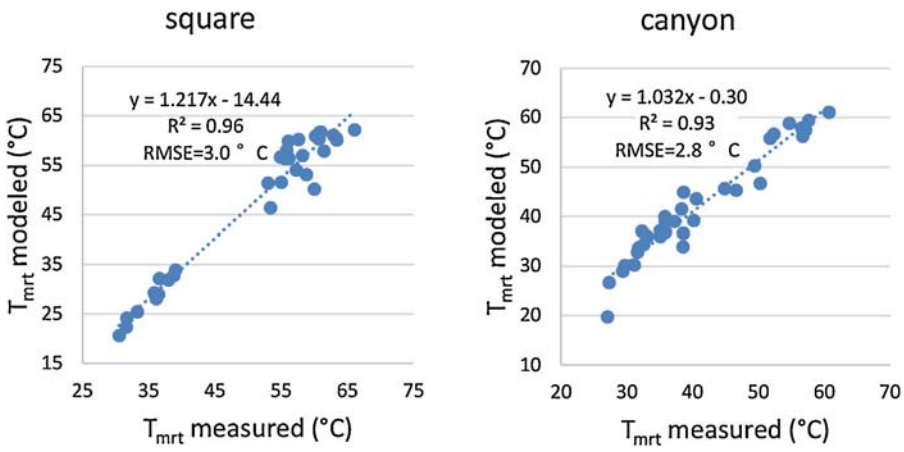

Fig. 7. Correlation between modeled and measured Tmrt at the two validation sites: (left) square case; (right) street canyon case.

Table 4
Statistics showing T_a, G, maximum T_{mrt} (max), minimum T_{mrt} (min), average T_{mrt} (avg) and standard deviation of T_{mrt} (std) for LJZ and XNM from 11:00 to 15:00.

Time	LJZ						XNM					
	T_a (°C)	G (W/m^2)	T_{mrt} (°C)				T_a(°C)	G(W/m^2)	T_{mrt} (°C)			
			max	min	avg	std			max	min	avg	std
11:00	36.1	894.5	83.9	40.9	62.7	12.5	37.0	894.5	73.3	45.4	64.2	6.9
12:00	37.5	972.2	84.4	46. 6	66.7	12.0	37.9	972.2	83.7	52.1	71.2	5.3
13:00	37.6	939.9	82.5	48.6	67.4	10.7	39.2	939.9	85.1	50.8	68. 8	6.7
14:00	38.0	763.2	84.4	50.8	66.5	13.1	40.1	763.2	90.0	52.1	70.4	6.3
15:00	38.7	601.3	74.8	46.3	59.3	6.2	39.0	601.3	79.0	46.4	61. 9	5.6

or trees. Minimum average T_{mrt} of 46.0 °C was found in the deep shadow casted by tall buildings and trees. The whole site's T_{mrt} values follow a normal distribution, with mean T_{mrt} value equal to 64.5 °C, and standard deviation equal to 7.9 °C. In comparison, the T_{mrt} values across XNM follow a similar normal distribution, but the curve is much steeper, with mean T_{mrt} value equal to 67.3 °C and standard deviation equal to 6.3 °C. The distribution patterns suggest that the spatial variation of T_{mrt} in XNM is less diverse as compared to LJZ, with larger proportion of higher T_{mrt} values. In fact, high T_{mrt} values above 70 °C were commonly found in street canyons.

To further examine the effect of urban geometry on the intra-urban differences of T_{mrt}, which includes building height and density, and street orientations and width, GIS-based spatial analysis modules were developed to distinguish urban spaces of different types, such as street canyon spaces, near building spaces and open spaces, and extract local T_{mrt} values for analysis. For LJZ, 3 types of urban spaces were identified, including north side of buildings which are within 10 m from a building's north-facing walls, south side of buildings which are within 10 m from a building's north-facing walls, and open spaces which are the places more than 100 m away from any buildings. Fig. 12 shows the statistical analysis result of the T_{mrt} values in the three types of urban spaces in LJZ. It shows that the majority of spaces in northern side of buildings have relatively low T_{mrt} values around 50–55 °C due to the shading by the buildings. In contrast, the T_{mrt} values in spaces in south side of buildings are much higher, with mean value equal to 63.6 °C, not only because of the incoming strong shortwave and longwave radiations, but also because of the intense radiations reflected from the sunlit south-facing walls. The spatial variation of T_{mrt} in open spaces far away from buildings shows a more diverse pattern, due to the highly varied shadow conditions created by buildings and trees. On the other hand, the mean value above 66 °C also suggests that open spaces are generally very hot in summer daytime.

For XNM, two types of urban spaces were identified, i.e. E-W street canyons and N-S street canyons. In practice, a tolerance angle of 30° was allowed so street canyons not exactly E-W or N-S oriented were also included. Fig. 13 shows the statistical analysis result of T_{mrt} values in E-W and N-S street canyons in XNM. It shows that T_{mrt} values in E-W street canyons are considerably higher than N-S street canyons, with a difference of 1.8 °C in the mean value. T_{mrt} is higher in E-W canyons mainly because the northern part of the canyons is normally sunlit and also close to sunlit south-facing walls. In contrast N-S street canyons especially narrow canyons are usually in shadow casted by buildings in the west. The result agrees with the findings in [39]. Another noticeable feature is that T_{mrt} values in E-W and N-S street canyons both follow normal distributions with majority values concentrating in the 60–70 °C range, reflecting the homogenously heat-dominant thermal radiant environment in street canyons.

The above discussions demonstrate that in different urban settings, the urban geometry plays an important role in affecting the local thermal radiant environment, as indicated by the spatial variation of T_{mrt}. It shows that, in urban environment with relatively open spaces with tall buildings such as LJZ, unobstructed open spaces have extremely high T_{mrt}. Near-building spaces in the southern side of buildings also have very high T_{mrt} which is influenced by both the ground surface and the south-facing walls. In contrast northern and western spaces of tall buildings tend to have lower T_{mrt} especially when trees are presented. In denser urban environment with low and moderate building height such as XNM, E-W street canyons especially the spaces in front of south-facing walls have very high T_{mrt}. Closed courtyards also have high T_{mrt} due to the lack of shading and also reflected shortwave radiation and longwave radiation from ground and wall surfaces, which is consistent

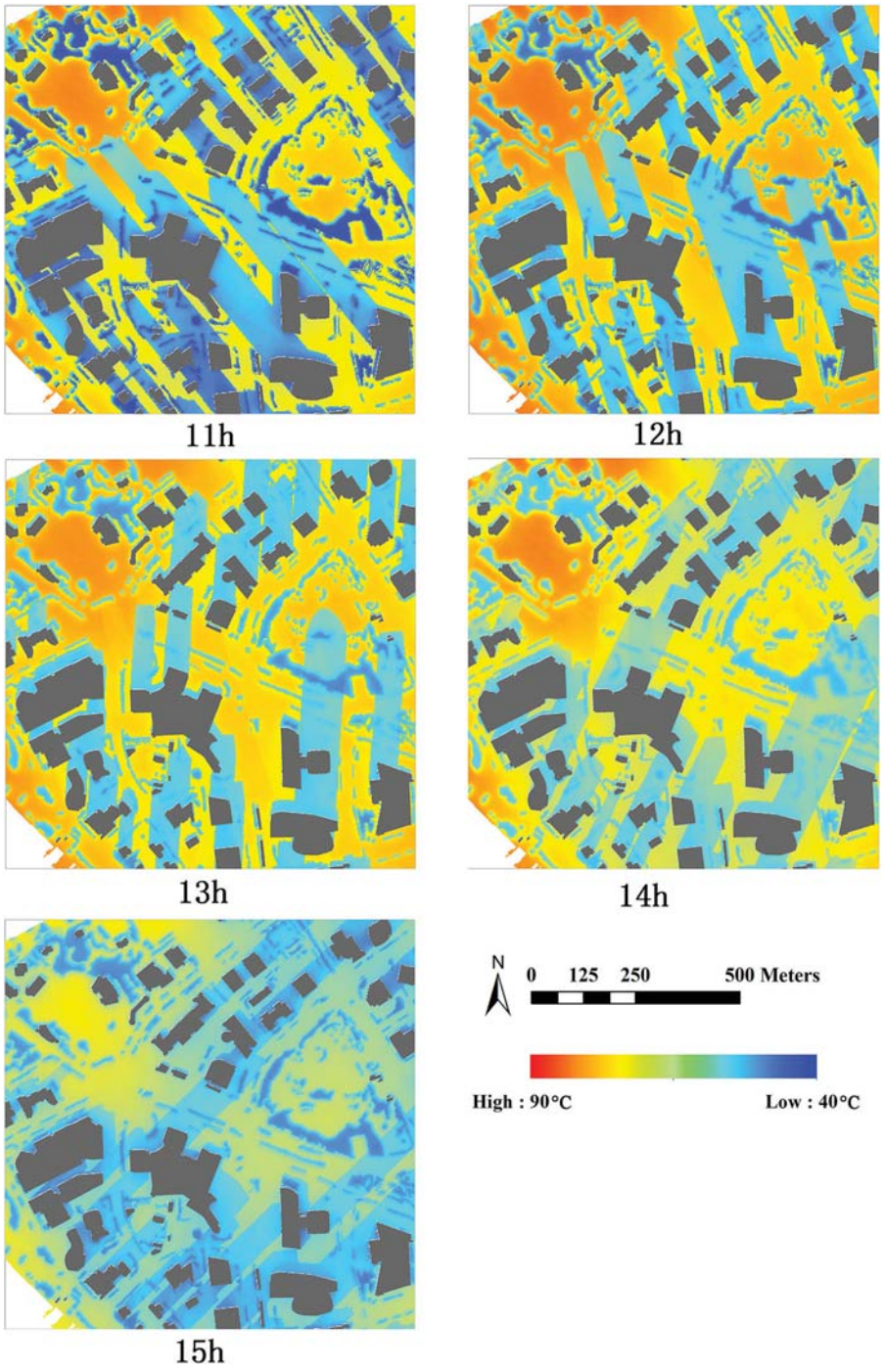

Fig. 8. Hourly Tmrt maps from 11:00 to 15:00 for LJZ.

with findings in the city of Gothenburg [36]. On the other hand, narrow N-S street canyons have lower T_{mrt} because of the abundant shading by surrounding buildings.

4.2. Implications for heat stress and countermeasures

Thorsson et al. [24] found that the T_{mrt} value of 59.4 °C is an important threshold value in predicting heat-related risk of mortality. In this study, the T_{mrt} value of 60 °C was considered as critical threshold value indicating the occurrence of heat stress in Shanghai. To consider both the intensity and duration of such heat stress induced by solar radiation, the index of Radiant Heat Stress Intensity (RHSI) was introduced, which is defined as the accumulative hourly difference of T_{mrt} above 60 °C for all the sun hours in a day, as given in Eq. (1) below.

$$\mathrm{RHSI} = \sum_{i=1}^{N} \begin{cases} {}^{T}\mathrm{mrt}(i) - 60\ ^{\circ}\mathrm{C}, & {}^{T}\mathrm{mrt}(i) > 60\ ^{\circ}\mathrm{C} \\ 0, & {}^{T}\mathrm{mrt}(i) \le 60\ ^{\circ}\mathrm{C} \end{cases} \quad (1)$$

where N is the total sun hours for that day, and $T_{mrt}(i)$ is the hourly average T_{mrt} value for the ith sun hour.

It was found that the RHSI range is 0–148.6 °C·hour for LJZ, and 0–137.6 °C·hour for XNM. The wide range suggests that even for spaces where heat stress occurred, large variation in terms of the lasting impact of heat stress can still be observed. In this sense, the

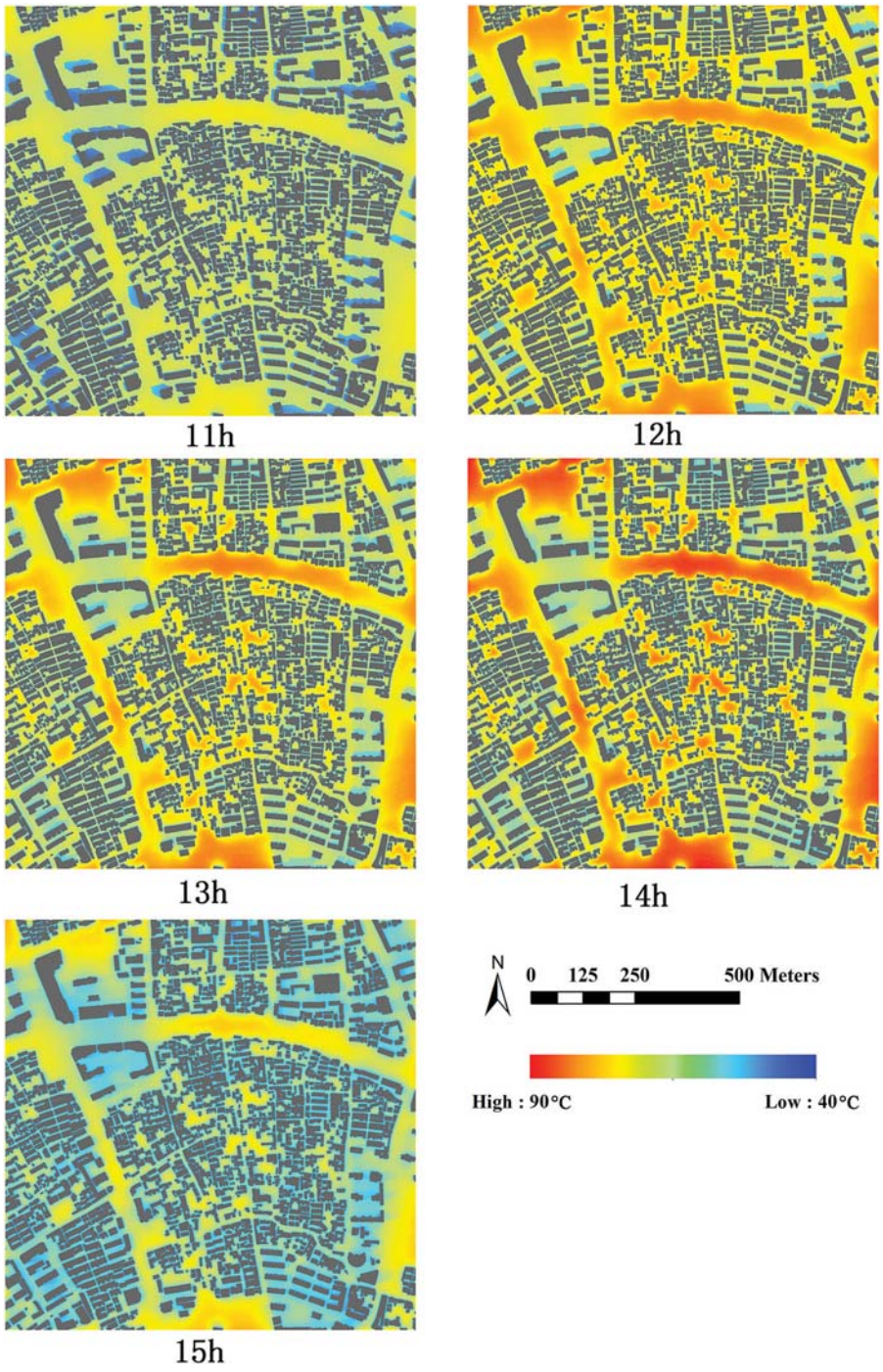

Fig. 9. Hourly Tmrt maps from 11:00 to 15:00 for XNM.

RHSI range was classified into 5 heat stress levels: 0–10 indicating low heat stress, 10–20 indicating moderate heat stress, 20–50 indicating high heat stress, 50–100 indicating very high heat stress, and 100 and above indicating heat extremes. Although there are other ways to select threshold values and define heat stress levels, the used method presents one logical and easy-to-interpret way to parameterize the spatial variations of the severity of heat stress in urban spaces. Fig. 14 shows the maps of RHSI classes in LJZ and XNM on the selected hot day, i.e. July 28, 2013.

The figure shows that paved open spaces in city center have the most severe heat stress, such as the large open squares in LJZ and the wide and unobstructed E-W roads in XNM. Such heat extremes are a combining effect of intense incoming and reflected shortwave radiation, longwave radiation from ground surface, and longer sun exposure. For example, some locations in the center of the large square in the northwest of LJZ could be under sunshine for more than 11 h a day, which induces extremely high heat stress. It was also observed that open spaces in the southern side of buildings can also have very high heat stress, which is affected by the reflected shortwave radiation from sunlit south-facing walls. On the other hand, low and moderate heat stress was found in the northern side of tall buildings where abundant shading was casted, and under tree canopies in urban green spaces. As one of the most prominent financial centers and tourist attractions in China, LJZ has a

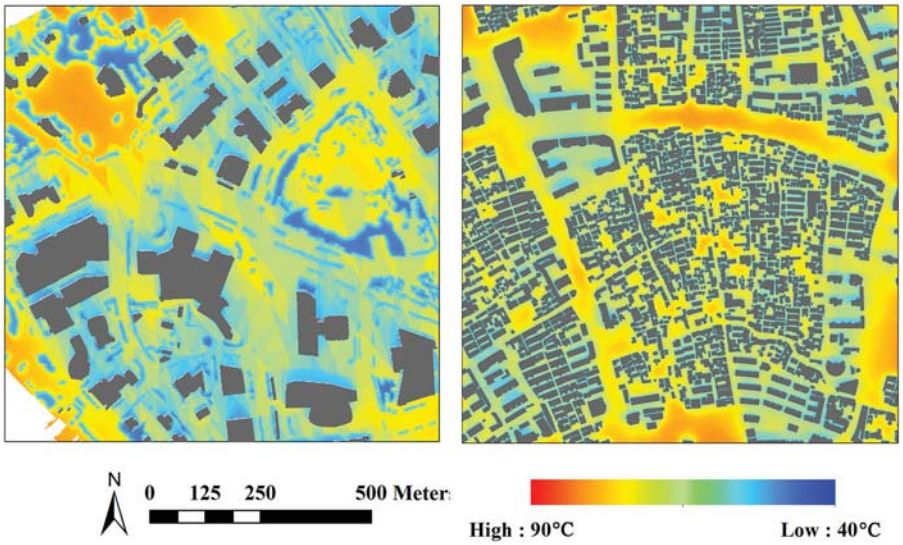

Fig. 10. Average hourly Tmrt maps from 11:00 to 15:00 of LJZ (left) and XNM (right).

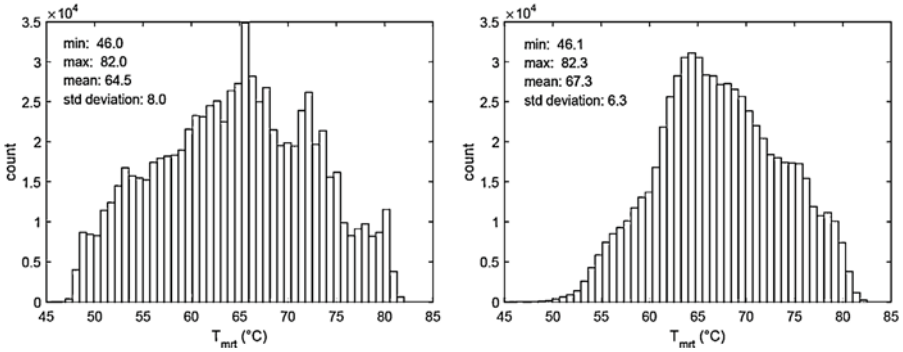

Fig. 11. Histograms of Tmrt values in two maps of LJZ (left) and XNM (right).

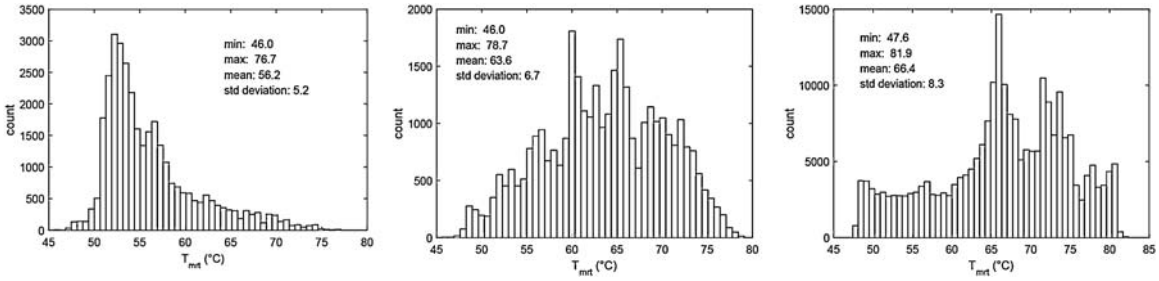

Fig. 12. Histograms of the statistics of Tmrt values in three types of urban spaces in LJZ: building north (left), building south (middle), and open space (right).

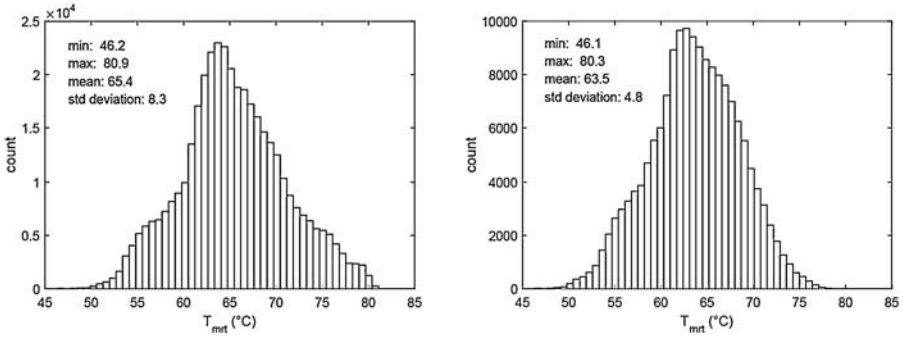

Fig. 13. Histograms of the statistics of Tmrt values in E-W (left) and N-S (right) street canyons in XNM.

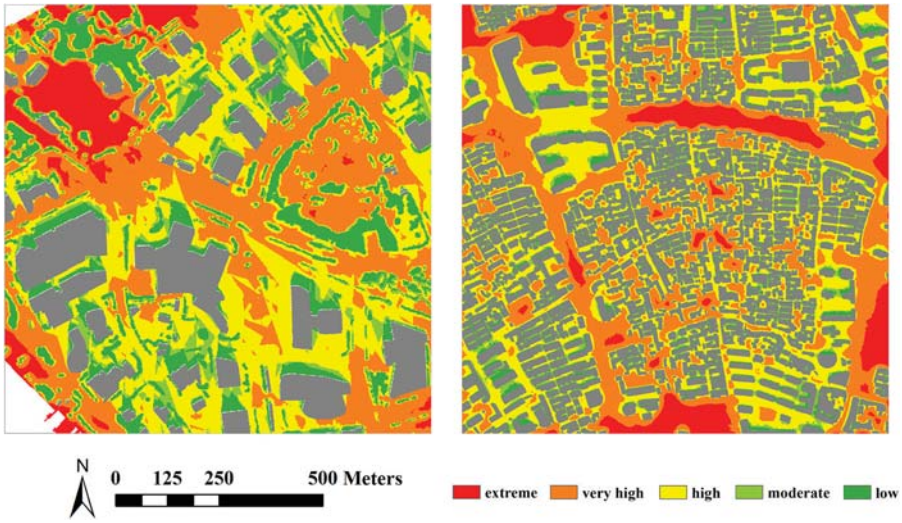

Fig. 14. RHSI class map on the simulation day for LJZ (left) and XNM (right).

lot of shopping centers, commercial office buildings and sightseeing spots located at different places. The very high heat stress in waterfront, squares and also spaces around buildings can be very unpleasant for pedestrians on hot summer days. Since the space between buildings is especially important for the local prosperity and vitality [48], effective shading devices, such as trees or kiosks should be provided for pedestrian spaces and major walkways in order to mitigate the local heat stress, which can benefit hundreds of thousands of office commuters and tourists every day in hot summer and therefore encourage the use of outdoor spaces. The large spacing between buildings should also be reduced to create denser urban fabrics and bring more shade to the spaces between buildings.

It was also found that in the denser urban environment of XNM, heat extremes also occurred in closed courtyards surrounded by densely packed low-rise buildings, which is primarily due to lack of shading, longer sun exposure, and also the effect of surrounding walls. Heat stress was normally more severe in E-W street canyons, with a vast majority having high heat stress, especially on the northern side of the streets which received less shading. Since XNM is dominated by old residential neighborhoods with a lot of senior citizens living around, these places with high heat stress are especially vulnerable to extreme climatic events such as heat waves. Due to the limited outdoor space in XNM, planting trees on the street may be hardly feasible. Therefore sunshades along walkways protecting pedestrians from direct sun exposure are the most effective measures to mitigate heat stress and improve pedestrians' thermal comfort. In contrast to E-W street canyons, N-S street canyons exhibited moderate heat stress or even low heat stress in some very narrow streets, suggesting that street orientations and building alignments could be appropriately controlled to mitigate heat stress in densely built-up areas, such as the design strategies proposed by [25,49,50]. Furthermore, recent studies also showed that retro-reflective materials applied to building facades and ground pavements have great potential in mitigating the surface heating in street canyons [51,52]. On the other hand, the use of shelters in narrow street canyons and modification of street orientations can also block the local ventilation, and it is also possible that retro-reflective ground and building surfaces may cause glare and lighting pollution. Therefore the countermeasures to mitigate heat stress should be evaluated against the local microclimatic and morphological context in order to achieve the best effect in terms of improving outdoor thermal comfort.

5. Conclusions

In this study, the intra-urban differences of T_{mrt} in Shanghai on a hot summer day were studied through a GIS-based simulation approach using the SOLWEIG model. The model was validated with integral radiant flux density measurements in Shanghai's summer climatic condition. Two different urban settings representing different urban fabrics in Shanghai's downtown center were selected as case studies. The RHSI index was defined to parameterize the impact of heat stress induced by solar radiation by considering both the intensity and duration of severe radiant heat. Heat stress areas were identified and classified based on the spatial variations of T_{mrt}. The results show that large open squares with little vegetation have the most severe heat stress, which is a result of long exposure to direct shortwave radiation. Spaces near sunlit south-facing walls and E-W street canyons also have very high heat stress, as a combing result of reflected shortwave radiation and longwave radiation from surrounding walls. Simple shading devices protecting pedestrians from direct sun exposure is the most effective way to immediately mitigate the local heat stress, and there are other design-level countermeasures such as reducing the spacing between buildings to introduce more shadow on walkways, re-designing street orientations to have more N-S street canyons, and also changing surface materials to reduce emitted longwave radiation from building walls. It is noteworthy that these strategies should be evaluated against other climatic aspects such as ventilation, and implemented in accordance with other design criteria in order to achieve a holistically optimized effect to improve pedestrian thermal comfort.

The study also reveals that spatial analysis based on continuous values over large spatial domains and consequent zonal understandings are substantially important for studying the intra-urban variation patterns in complex urban environment. These analysis and understandings are only possible when spatial information is present, therefore the support of GIS is essential to the research objectives. On the other hand, one limitation of the present study is that different ground cover characteristics, such as grassland were not considered in the simulations, and further investigations including more land cover types are required in future work.

Acknowledgements

This study is jointly supported by the National Natural Science Foundation of China (Nos.: 41301087; 41471449), the Natural

Science Foundation of Shanghai (No. 14ZR1412200) and Innovation Program of Shanghai Municipal Education Commission (No.: 15ZZ020). Special thanks are due to Miss Yan Huang and Miss Junhan Wu for the assistance in figure editing. The authors would also like to thank the two reviewers for their pertinent comments and suggestions of some of the most up-to-date related papers, which contribute largely to the improvement of this paper.

References

[1] M. Santamouris, N. Papanikolaou, I. Livada, I. Koronakis, C. Georgakis, A. Argiriou, D.N. Assimakopoulos, On the impact of urban climate on the energy consumption of buildings, Sol. Energy 70 (3) (2001) 201–216.
[2] M. Santamouris, On the energy impact of urban heat island and global warming on buildings, Energy Build. 82 (2014) 100–113.
[3] F. Rossi, E. Bonamente, A. Nicolini, E. Anderini, F. Cotana, A carbon footprint and energy consumption assessment methodology for UHI-affected lighting systems in built areas, Energy Build. 114 (2016) 96–103.
[4] L. Chen, E. Ng, Outdoor thermal comfort and outdoor activities: a review of research in the past decade, Cities 29 (2012) 118–125.
[5] S. Hajat, M. O'Connor, T. Kosatsky, Health effects of hot weather: from awareness of risk factors to effective health protection, Lancet 375 (2010) 856–863.
[6] K.M.A. Gabriel, W.R. Endlicher, Urban and rural mortality rates during heat waves in Berlin and Brandenburg, Germany, Environ. Pollut. 159 (2011) 2044–2050.
[7] W.B. Goggins, E.Y.Y. Chan, E. Ng, C. Ren, L. Chen, Effect modification of the association between short-term meteorological factors and mortality by urban heat islands in Hong Kong, PLoS One 7 (2012) e38551.
[8] A.J. Arnfield, Review: two decades of urban climate research: a review of turbulence, exchanges of energy and water, and the urban heat island, Int. J. Climatol. 23 (2003) 1–26.
[9] I. Stewart, A systematic review and scientific critique of methodology in modern urban heat island literature, Int. J. Climatol. 31 (2011) 200–217.
[10] H. Takebayashi, M. Moriyama, Surface heat budget on green roof and high reflection roof for mitigation of urban heat island, Build. Environ. 42 (2007) 2971–2979.
[11] Z. Tan, K.K.-L. Lau, E. Ng, Urban tree design approaches for mitigating daytime urban heat island effects in a high-density urban environment, Energy Build. 114 (2016) 265–274.
[12] Y. Wang, U. Berardi, H. Akbari, Comparing the effects of urban heat island mitigation strategies for Toronto, Canada, Energy Build. 114 (2016) 2–19.
[13] M. Santamouris, Cooling the cities—a review of reflective and green roof mitigation technologies to fight heat island and improve comfort in urban environments, Sol. Energy 103 (2014) 682–703.
[14] H. Akbari, C. Cartalis, D. Kolokotsa, A. Muscio, A.L. Pisello, F. Rossi, M. Santamouris, A. Synnefa, N.H. Wong, M. Zinzi, Local climate change and urban heat island mitigation techniques—the state of the art, J. Civ. Eng. Manag. 22 (2016) 1–16.
[15] P.O. Fanger, Thermal Comfort Analysis and Application in Environment Engineering, McGraw Hill Book Company, New York, 1972.
[16] ASHRAE, ASHRAE Fundamentals Handbook 2001 (SI Edition), Atlanta, USA: GA, 2001.
[17] H. Mayer, P. Höppe, Thermal comfort of man in different urban environments, Theor. Appl. Climatol. 38 (1987) 43–49.
[18] W. Koch, Relationship between air temperature and mean radiant temperature in thermal comfort, Nature 196 (1962) 587.
[19] P. Höppe, A new procedure to determine the mean radiant temperature outdoors (in German), Wetter Leb. 44 (147–151) (1992).
[20] S. Masmoudi, S. Mazouz, Relation of geometry,vegetation and thermal comfort around buildings in urban settings, the case of hot arid regions, Energy Build. 36 (7) (2004) 710–719.
[21] S. Thorsson, M. Lindqvist, S. Lindqvist, Thermal bioclimatic conditions and patterns of behaviour in an urban park in Goteborg, Int. J. Biometeorol. 48 (2004) 149–156.
[22] R. Emmanuel, H. Rosenlund, E. Johansson, Urban shading—a design option for the tropics? A study in Colombo, Sri Lanka, Int. J. Climatol. 27 (2007) 1995–2004.
[23] N. Kántor, J. Unger, The most problematic variable in the course of human-biometeorological comfort assessment—the mean radiant temperature, Cent. Eur. J. Geosci. 3 (1) (2011) 90–110.
[24] S. Thorsson, J. Rocklöv, J. Konarska, F. Lindberg, B. Holmer, B. Dousset, D. Rayne, Mean radiant temperature—A predictor of heat related mortality, Urban Clim. 10 (2) (2014) 332–345.
[25] F. Ali-Toudert, F.H. Mayer, Effects of asymmetry galleries, overhanging facades and vegetation on thermal comfort in urban street canyons, Sol. Energy 81 (2007) 742–754.
[26] Hyunjung Lee, Jutta Holst, Helmut Mayer, Modification of human-biometeorologically significant radiant flux densities by shading as local method to mitigate heat stress in summer within urban street canyons, Adv. Meteorol. 2013 (2013), http://dx.doi.org/10.1155/2013/312572, Article ID 312572, 13 pages.
[27] H. Lee, H. Mayer, L. Chen, Contribution of trees and grasslands to the mitigation of human heat stress in a residential district of Freiburg, Southwest Germany, Landsc. Urban Plan. 148 (2016) 37–50.
[28] A. Chatzidimitriou, S. Yannas, Microclimate development in open urban spaces: the influence of form and materials, Energy Build. 108 (2015) 156–174.
[29] D. Lai, C. Zhou, J. Huang, Y. Jiang, Z. Long, Q. Chen, Outdoor space quality: a field study in an urban residential community in central China, Energy Build. 68 (B) (2014) 713–720.
[30] H. Radhi, F. Fikry, S. Sharples, Impacts of urbanisation on the thermal behaviour of new built up environments: a scoping study of the urban heat island in Bahrain, Landsc. Urban Plan. 113 (2013) 47–61.
[31] C. Ketterer, A. Matzarakis, Human-biometeorological assessment of heat stress reduction by replanning measures in Stuttgart, Germany, Landsc. Urban Plan 122 (2014) 78–88.
[32] S.-R. Yang, T.-P. Lin, An integrated outdoor spaces design procedure to relieve heat stress in hot and humid regions, Build. Environ. 99 (2016) 149–160.
[33] F. Lindberg, S. Thorsson, D. Rayner, K. Lau, The impact of urban planning strategies on heat stress in a climate-change perspective, Sustain. Cities Soc. 25 (2016) 1–12.
[34] F. Yang, L. Chen, Developing a thermal atlas for climate-responsive urban design based on empirical modeling and urban morphological analysis, Energy Build. 111 (2016) 120–130.
[35] F. Lindberg, C.S.B. Grimmond, The influence of vegetation and building morphology on shadow patterns and mean radiant temperatures in urban areas: model development and evaluation, Theor. Appl. Climatol. 105 (2011) 311–323.
[36] K.K.-L. Lau, F. Lindberg, D. Rayner, S. Thorsson, The effect of urban geometry on mean radiant temperature under future climate change: a study of three European cities, Int. J. Biometeorol. 59 (7) (2015) 799–814.
[37] E. Erell, D. Pearlmutter, D. Boneh, P. Kutiel, Effect of high-albedo materials on pedestrian heat stress in urban street canyons, Urban Clim. 10 (2014) 367–386.
[38] F. Lindberg, S. Onomura, C.S.B. Grimmond, Influence of ground surface characteristics on the mean radiant temperature in urban areas, Int. J. Biometeorol. 60 (9) (2016) 1439–1452.
[39] K.K.-L. Lau, C. Ren, J. Ho, E. Ng, Numerical modelling of mean radiant temperature in high-density sub-tropical urban environment, Energy Build. 114 (2016) 80–86.
[40] F. Lindberg, B. Holmer, S. Thorsson, SOLWEIG 1.0—modelling spatial variations of 3D radiant fluxes and mean radiant temperature in complex urban settings, Int. J. Biometeorol. 52 (7) (2008) 697–713.
[41] ShanghaiDaily, Official 40.6 °C Makes It Another Record Day for City, 2016, Retrieved from: http://www.shanghaidaily.com/Metro/society/An-official-406C-makes-it-another-record-day-for-city/shdaily.shtml (Last accessed 2.06.16).
[42] BBC, China Issues Heat Alert as 'Hottest July' Hits Shanghai, 2016, Retrieved from: http://www.bbc.com/news/world-asia-china-23499175 (Last accessed 2.06.16).
[43] S. Thorsson, F. Lindberg, B. Holmer, I. Eliasson, Different methods for estimating the mean radiant temperature in an outdoor urban setting, Int. J. Climatol. 27 (14) (2007) 1983–1993.
[44] M. Bruse, H. Fleer, Simulating surface-plant-air interactions inside urban environments with a three-dimensional numerical model, Environ. Modell. Softw. 3 (1998) 373–384.
[45] A. Matzarakis, F. Rutz, H. Mayer, Modelling radiation fluxes in simple and complex environments—application of the RayMan model, Int. J. Biometeorol. 51 (4) (2007) 323–334.
[46] Y.-C. Chen, T.-P. Lin, A. Matzarakis, Comparison of mean radiant temperature from field experiment and modelling: a case study in Freiburg, Germany, Theor. Appl. Climatol. 118 (2014) 535–551.
[47] Y. Huang, B. Yu, J. Zhou, C. Hu, W. Tan, Z. Hu, J. Wu, Toward automatic estimation of urban green volume using airborne LiDAR data and high resolution remote sensing images, Front. Earth Sci. 7 (1) (2013) 43–54.
[48] J. Gehl, Life Between Buildings: Using Public Space, 6th ed., Island Press, 2011.
[49] H. Andrade, M.-J. Alcoforado, Microclimatic variation of thermal comfort in a district of Lisbon (Telheiras) at night, Theor. Appl. Climatol. 92 (3–4) (2008) 225–237.
[50] S. Thorsson, F. Lindberg, J. Björklund, B. Holmer, D. Rayner, Potential changes in outdoor thermal comfort conditions in Gothenburg, Sweden due to climate change: the influence of urban geometry, Int. J. Climatol. 31 (2011) 324–335.
[51] F. Rossi, B. Castellani, A. Presciutti, E. Morini, M. Filipponi, A. Nicolini, M. Santamouris, Retro reflective façades for urban heat island mitigation: experimental investigation and energy evaluations, Appl. Energy 145 (2015) 8–20.
[52] F. Rossi, B. Castellani, A. Presciutti, E. Morini, E. Anderini, M. Filipponi, A. Nicolini, Experimental evaluation of urban heat island mitigation potential of retro-reflective pavement in urban canyons, Energy Build. 126 (2016) 340–352.